

**Structural transitions in two-dimensional hard-sphere systems**

S. C. Wu, D. T. Wasan,\* and A. D. Nikolov

*Department of Chemical and Environmental Engineering, Illinois Institute of Technology, Chicago, Illinois 60616, USA*

(Received 20 January 2004; revised manuscript received 8 November 2004; published 20 May 2005)

We spread randomly noncharged steel particles (diameter, 1.59 mm) on a silicon wafer to form a two-dimensional hard-sphere system. The particle structure versus the particle coverage was monitored. We observed the particle structural transition from liquidlike to triangular-lattice crystal-like with increasing particle coverage by analyzing the particle structure factor. The particle coverage at which the structural transition occurs was quantified by the curves of  $S_{\max}(A)$  and  $G_6(A)$ ;  $S_{\max}$  is the amplitude of the first peak of the structure factor (depicting the particle positional order), and  $G_6$  is the bond orientation order parameter. We also conducted a Monte Carlo simulation study. The Monte Carlo simulation results show good agreement with the experimental results at low particle area fractions. However, at high area fractions, the experimentally observed particle structure is less organized than that generated by simulations.

DOI: 10.1103/PhysRevE.71.056112

PACS number(s): 64.60.Cn, 64.70.-p

**I. INTRODUCTION**

Structural transitions in two-dimensional (2D) systems are of great interest to scientists for a number of different reasons. Fundamental physics explores the influence of the degree of freedom on the structural transitions. The character of the particle structural transitions in two-dimensional systems for specific model fluids has attracted considerable interest [1–3]. We will concentrate on studying the “hard-sphere” structural transition. The hard-sphere model is characterized by a pair interaction potential that is zero except at distances smaller than at contact, where it becomes infinitely repulsive. The hard-sphere system has been studied analytically [4] and through computer simulations [5]; it has been used extensively as a reference system [6] in simple fluid theories. A basic understanding of a hard-sphere system is important since it provides a starting point for the successful perturbation theory of liquids developed by Barker and Henderson [7]. The hard-sphere structural transitions occur in the many-body system and are driven by the entropy effect.

In 1960, Turnbull and Cormia [8] developed a dynamic two-dimensional hard-sphere model to observe structural transitions. In this model, many uniform glass hard spheres were moved steadily and at random on a horizontal circular glass plate. The sphere structure transitions were observed via high-speed photographs of the spheres in motion. The model exhibited a “gaslike” state at a low sphere density. As the density increased, the behavior became more “liquidlike” and then “crystallization” occurred. Section V, “Discussion,” has the analysis of their photographs; we found their results to be in good agreement with our hard-sphere experiment.

In 1978 and 1984, Pieranski *et al.* [9] placed steel particles on the plastic plate of a hexagonal box. The structural transition versus particle coverage was studied qualitatively using a photographic technique to record images of the pair distribution function. The authors argued that they observed

the coexistence of solidlike and fluidlike structures. Their observation of the particle structural transition is in agreement with the computer simulation data of Alder and Wainwright [10]. However, one can argue that the experiment conducted by Pieranski *et al.* is not a hard-sphere system. Steel particles rubbing on a plastic surface acquire positive charges and leave negative charges on the plastic surface [11].

More recently, physicists have recognized granular matter used in Refs. [8,9] as a paradigm for “driven,” dissipative systems far from equilibrium [12]. There are two particularly important aspects that contribute to the unique properties of granular materials, ordinary temperature plays no role, and the interactions between granular particles are dissipative because of static friction and the inelasticity of collisions [13,14]. The driven granular medium reaches a steady state, where the energy lost through collisions is balanced by the amount added externally [15]. One of the most fascinating peculiarities of granular matter is their transition from a fluidlike to a solidlike (disordered to ordered). The fluidlike-solidlike transition for vertically vibrated monolayers has been demonstrated by changing the amount of mechanical energy flowing into the granule [16,17]. Straßburger and Rehberg [18] studied the granular transition from randomly arranged to crystallike structure on a horizontally vibrated plate by increasing the particle filling fraction. The importance in granular transition has been stressed in connection with the coagulation of planetesimals into planets [19]. The granular material has tremendous importance for industrial processes in areas ranging from agriculture to civil engineering to pharmaceutical processing. There has been a long-standing interest in describing and predicting the phenomena of granular materials [20]. However, despite much effort, there still is no comprehensive understanding as exists for other forms of matter like ordinary fluids or solids [12].

Based on the computer simulation data, Alder and Wainwright [10] studied the melting transition in hard-disc systems. From the observation of a “loop” in the area fraction occupied by the disks vs pressure curve, they concluded that the phase transition is of the first order. These findings were essentially confirmed by subsequent investigations by

---

\*Author to whom correspondence should be addressed. Email address: wasan@iit.edu

Hoover and Ree [21]. However, the effects of the finite sizes of the simulated systems in these early studies were not examined in a quantitative way. Zollweg and Chester [22] revealed that the tie line (coexistence of a liquid and solid) is indeed much shorter than previously observed by using larger systems with more particles. They concluded that the tie line might become even shorter, or vanish entirely, if the system size increased. Weber, Marx and Binder [23] used a finite-size scaling method to determine the order of the particle transition and to obtain the bounds of the transition density by measuring the bond orientation order parameter, its susceptibility, and compressibility. They claim to have found the evidence of the first-order phase transition.

The nature of the 2D particle structural transition is still unresolved. The Kosterlitz-Thouless-Halperin-Nelson-Young (KTHNY) theory predicts 2D solids might melt via two continuous phase transitions with an intervening phase termed “hexatic”—between a liquid and a solid phase. However, Ryzhov and Tareyeva [24] carried out density functional calculations to obtain first-principles estimates for the stability limits of a hard-disk solid and a hexatic phase. Their results ruled out the existence of a hard-disk hexatic.

We conducted the following work to reveal the structural transition of a 2D hard-sphere system versus the particle coverage. This paper is organized as follows: in Sec. II, we describe the experimental material and setup. We describe the computer simulation method used in this paper in Sec. III. In Sec. IV (Results), we describe the data analysis procedure; present the results of our experiment through the structure factor and bond orientation order parameter. In Sec. V (Discussion), the results of our work are compared with those in the literature. Our Monte Carlo simulation results are also described. The 2D hard-sphere structures from the computer simulation and the granular system are compared. The structural transition phenomena are discussed in detail; we summarize the paper in Sec. VI.

## II. EXPERIMENT

### A. Materials

We used nonmagnetized stainless-steel particles (diameter, 1.59 mm; type, 316L; Grade, 100; Thompson Precision Ball Co., USA). The steel particles were kept in a metal container to discharge them. We soaked the particles in toluene for 4 to 5 hours and washed them with fresh toluene; these cleaned particles were vacuum-dried for 30 minutes. The particles were transferred to a silicon wafer and immediately covered with a culture dish to minimize the exposure to the atmosphere. The silicon wafer had a molecular-smooth surface and was 10 cm in diameter (Silicon Valley Microelectronics, USA). We removed all debris from the silicon wafer with an air duster (Fellowes, USA) before each experiment.

### B. Experimental setup

The operating conditions were maintained at 25 °C and the relative humidity was less than 50%. We prepared the 2D system by spreading a monolayer of a few thousand stainless

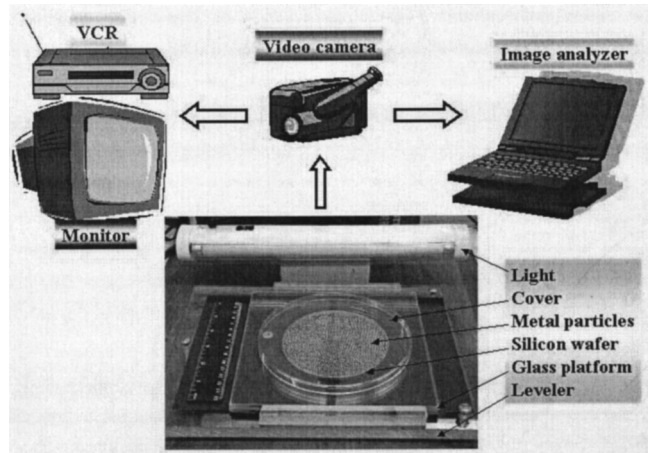


FIG. 1. Design used to study structural transitions. Stainless steel particles (diameter, 1.59 mm) were spread on the surface of a silicon wafer. The particles were filmed by a video camera and analyzed by the image software Image-Pro.

steel particles on the surface of a silicon wafer (Fig. 1). The silicon wafer was placed horizontally on the center hole of a set of glass plates and covered by a polystyrene culture dish. We shook the glass platform to make the metal particles move randomly on the silicon wafer surface. The shaking was a combination of reciprocal and orbital vibration in horizontal direction with frequency of about 6 Hz and amplitude of about 1 mm. We varied the area fraction of the metal particles,  $A$  (the area occupied by metal particles divided by the total system area), to study the ordering behavior in the system. For  $n$  particles of diameter  $d$  in the system of area  $S$ ,  $A$  is defined as  $A = (n\pi d^2)/(4S)$ . We examined the ordering behavior of the metal particles by varying  $A$  from 0.37 to 0.84. The particles' motions were recorded at 30 frames per second by a video camera under suitable lighting conditions. The images represent quenched configurations. Figure 2 shows two typical configurations at  $A=0.54$  and 0.84. The video camera was connected to a monitor and VCR for monitoring and recording the images. The particle configurations were digitized by image analysis software (Image-Pro Plus, USA) for further investigation.

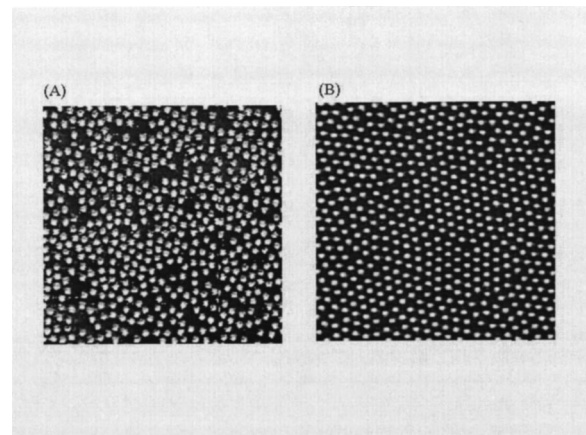


FIG. 2. Monitoring the particle positions at different particle area fractions, (A)  $A=0.54$ , (B)  $A=0.84$ .

The particle charge was quantified using the method described by Tata *et al.* [11]. The particles placed on the wafer were shaken (to create a charge on the particles). Then the wafer was declined at a small angle (less than 10 degree), and the positions of the particles were monitored. The repulsion between the particles corresponded to the balance between the Coulomb and gravitational forces. The charge was estimated by monitoring the particle distance versus the angle. This method of measuring charge particle is accurate to 0.01 esu; no charge was detected on the steel particles (at the area fractions between 0.37 and 0.84).

### III. MONTE CARLO SIMULATION

We used the hard-disc Monte Carlo simulation to compare the results of our experiment with the computer simulation. The Metropolis algorithm [25] was used to obtain the equilibrium in a canonical ensemble (constant  $NVT$  ensemble) [6]. The use of periodic boundary conditions eliminates the boundary effects. The basic simulation cell length,  $L$ , is fixed according to  $L^2 = (n\pi d^2)/(4A)$  to get the required particle area fraction  $A$ , where  $d$  is the diameter of hard disc and is the same as the diameter of the metal particles used in experiment. The particle number was fixed at  $n=484$  except during the structural transition, and  $n$  was 1024 at the transition area fraction. According to the analysis of the 2D size-dependent properties proposed by Zollweg *et al.* [22], the difference in pressure for 2D systems with  $n=256$  and  $n=16384$  is smaller than 0.1%.

The particle area fraction range in our simulations is  $A=0.37$  to  $0.78$ . The system was allowed to evolve with Monte Carlo trajectories. Approximately 30 000 sweeps were initially discarded (one sweep is an attempted move per particle). The system evolved rapidly toward equilibrium during this process. Structural functions, like the radial distribution function  $g(r)$  and the structure factor  $S(Q)$ , were monitored to ascertain if equilibrium had been reached. Our averaging was done over 30 000 sweeps when the system area fraction was out of the structural transition range. When the system area fraction was close to the structural transition range,  $A \sim 0.65$ – $0.85$ , the averaging was done over 60 000 sweeps.  $g(r)$  is calculated with a small interval,  $\Delta r=0.01d$ , and  $S(Q)$  is calculated with  $\Delta Qd=0.1$ , using the standard method [26].

## IV. EXPERIMENTAL RESULTS

### A. Structure factor

In order to obtain information about particle structures, the structure factor was calculated from radial distribution function. Radial distribution function,  $g(r)$ , is the probability of observing a particle at distance  $r$  from a given particle. To avoid the effect of wall on particle structure [18], we select the center region of about  $40d$  by  $40d$  from original image. The whole  $g(r)$  curve, except the first peak amplitude  $g_{\max}$ , depends little on the interval width  $\Delta r$ ; we chose  $\Delta r=0.1d$ . We explored the particle structure through the structure factor  $S(Q)$  and the structural ordering parameter  $S_{\max}$  derived from it, because  $g_{\max}$  is sensitive to the  $\Delta r$ . The structure

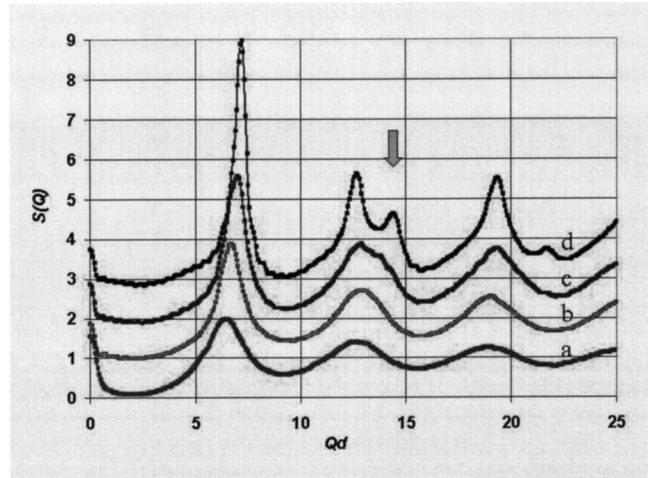


FIG. 3. Structure factor  $S(Q)$  of experimental metal particles on the silicon surface at different area fractions of  $A$ . Curves  $a$ ,  $b$ ,  $c$ , and  $d$  correspond to  $A=0.54$ ,  $0.67$ ,  $0.77$ ,  $0.84$ , respectively. Curves  $b$ ,  $c$ , and  $d$  are shifted vertically for clarity. The boldface arrow shows the appearance of the triangular lattice.

factor characterizes the changes in the local density as a result of the external fields of the spatial frequency  $Q=2\pi/\lambda$ , where  $\lambda$  is the corresponding wavelength [27]. The structure factor  $S(Q)$  is obtained from the Fourier transform of  $g(r)$  by [28]

$$S(Q) = 1 + \rho \int [g(r) - 1] e^{-i\vec{Q}\cdot\vec{r}} d\vec{r}, \quad (1)$$

where  $\rho$  is the particle's 2D density related to the area fraction  $A$  by  $A=\rho\pi d^2/4$ . Equation (1) can be written in the two-dimensional form as

$$S(Q) = 1 + \rho \int r [g(r) - 1] \cos(-Qr \cos \theta) d\theta dr, \quad (1')$$

where  $\theta$  is the integration parameter of angle.

The variation of the first peak amplitude of  $S(Q)$ ,  $S_{\max}$ , on both the distance intervals  $\Delta r/d$  and spatial frequency intervals  $\Delta Qd$  is within 1%. We choose  $\Delta r=0.1d$  and  $\Delta Qd=0.06$  for the following analysis of  $S(Q)$  and  $S_{\max}$ . Figure 3 shows the curves of  $S(Q)$  obtained at several different area fractions. The structure factor curves show oscillatory decay with spatial frequency,  $Qd$ , for every area fraction. The peak positions are at the multiples of  $Qd \sim 2\pi$  for the hard-sphere interactions. The amplitudes of the maximum and minimum increase as the area fraction increases. The second peak forms a small bump at  $A=0.77$ , then splits between the area fractions  $A=0.77$  and  $A=0.84$ . This is characteristic of triangular-lattice formation [1,18,29,30].

The maxima of  $S(Q)$  are analogues of Bragg peaks in the crystal diffraction pattern. The first maximum,  $S_{\max}$ , is the index of the density susceptibility at the nearest neighboring particle. The structural transition has been identified from the sudden change in the  $S_{\max}$  behavior as a function of the area fraction,  $A$  [31]. Our experimental data show that the  $S_{\max}$  reflects less error and is a more accurate method to quantify the particle structural transition than  $g_{\max}$  [32]. We obtained

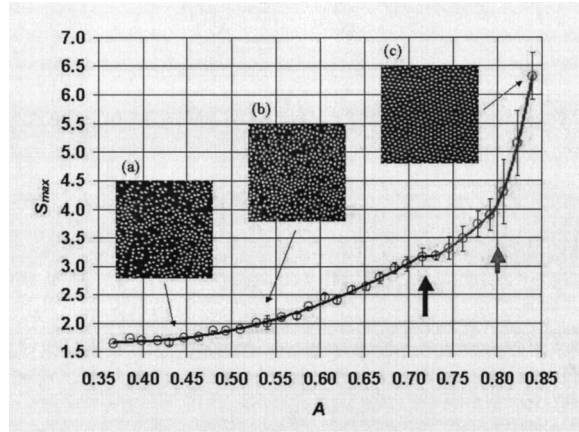


FIG. 4.  $S_{\max}$  vs  $A$  for experimental metal particles on the silicon surface. A plateau appears at approximately  $A=0.72-0.73$  and  $S_{\max}=3.2$  (long boldface arrow). Sudden increases of  $S_{\max}$  accompanied with more scattering appear at approximately  $A=0.80$  and  $S_{\max}=4$  (short boldface arrow). Insets are particle configurations corresponding to (a)  $A=0.44$ , (b)  $A=0.54$ , and (c)  $A=0.84$ .

the structural parameter  $S_{\max}$  from the amplitude of the first peak of  $S(Q)$  at each area fraction.

Figure 4 shows the trend of  $S_{\max}$  as a function of the area fraction,  $A$ , with the particle photography shown in the inset. The  $S_{\max}$  increases with the increasing  $A$ . However, a small plateau occurred at  $A=0.72-0.73$ ; and beyond the plateau, the scatterings in  $S_{\max}$  were found to be larger. The slope of  $S_{\max}$  increases suddenly after  $A$  reaches 0.80, and is accompanied with more scattering than in the other regions. The scattering reaches a maximum at  $A=0.81-0.82$  and then decreases again.

### B. Bond orientation order parameter

The second peak of the  $S(Q)$  curves (Fig. 3) splits into two peaks when the area fraction increases from 0.77 to 0.84. The splitting occurs at the characteristic distance of triangular lattice. The particle structural evolution from disorder to order in the triangular lattice motivated us to use the bond orientation order parameter with sixfold symmetry,  $G_6$ , to quantify the structural transitions in 2D systems. Here, “bond” denotes the imaginary line connecting the centers of two neighboring particles. A configuration possesses a bond-orientation order if the angles between these bonds and an arbitrary fixed axis are correlated. Mermin [33] found that although true positional order implies bond-orientation order, the latter could exist without the former.

The particle structural transition was observed through the positional order parameter  $S_{\max}$  vs  $A$ . We will now discuss the bond orientation order parameter  $G_6$  vs  $A$  to gain an understanding of the structural transition [34].  $G_6$  is defined as

$$G_6 = \frac{1}{N_f} \sum_{j=1}^{N_f} \left| \frac{1}{n_j} \sum_{p=1}^{n_j} \left( \frac{1}{m_p - 1} \sum_{k=1}^{m_p - 1} e^{i6\Delta\theta_{kp}} \right) \right|, \quad (2)$$

where the sums are over the number of the frames  $N_f$ , the number of particles  $n_j$  in the  $j$ th frame, and the number of

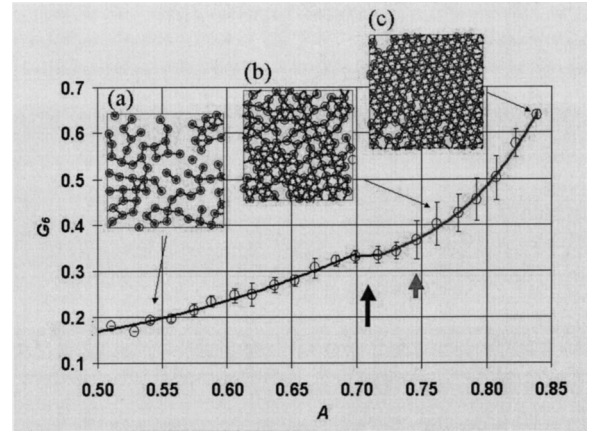


FIG. 5.  $G_6$  vs  $A$  for experimental metal particles on the silicon surface. A plateau appears at approximately  $A=0.70-0.72$  and  $G_6=0.32$  (long boldface arrow).  $G_6$  increases rapidly after the plateau and is accompanied by large scattering after  $A=0.74$  and  $G_6=0.38$  (short boldface arrow). Insets are the particle bonds within the region of  $10d$  by  $10d$  corresponding to (a)  $A=0.54$ , (b)  $A=0.77$ , and (c)  $A=0.84$ .

neighbors  $m_p$  of the  $p$ th particle.  $\Delta\theta_{kp}$  is the angle difference between the bonds connecting particles  $k$  and  $p$ .  $G_6$  is an index of the ratio of particles forming the triangular lattice and is 1 for the pure triangular lattice. We first calculate the number of neighboring particles and bonding for each particle, and then determine the value of the bond orientation order parameter.

The particle neighbors were determined by the following rule. The triangular-lattice bond is formed when the particle separation is smaller than 1.152 particle diameters,  $d$  [35], which is the smallest particle separation when a particle has seven neighbors (hard-sphere interactions). A bond is a virtual line that is a representation of particle interactions. The experimental particle bonds (within the region of  $10d$  by  $10d$  at  $A=0.54, 0.77, 0.84$ ) are shown in the insets of Fig. 5. (The circles show the schematic of the particles that do not have proportional particle diameters. The dots inside the circles are the centers of the particles. The lines connecting particle centers are the determined bonds.) More bonds are formed as the area fraction,  $A$ , increases. The particle structure formed by the bonds is a combination of square and triangular symmetry at  $A=0.77$  in Fig. 5(b). The particles form a triangular lattice with some structural defects inside the lattice at the ordered structure with an area fraction of  $A=0.84$  in Fig. 5(c).

Figure 5 shows the bond orientation order parameter,  $G_6$ , as a function of the area fraction,  $A$ . The  $G_6$  increases with an increasing  $A$ . There is a small plateau in the experimental curve at  $A=0.70-0.72$ , similar to that of  $S_{\max}$  vs  $A$ .  $G_6$  rapidly increases after the plateau and is accompanied by larger scatterings.

## V. DISCUSSION

The  $S(Q)$ ,  $S_{\max}(A)$ , and  $G_6(A)$  were analyzed to rationalize the results of the experiment. Figure 3 shows the experi-

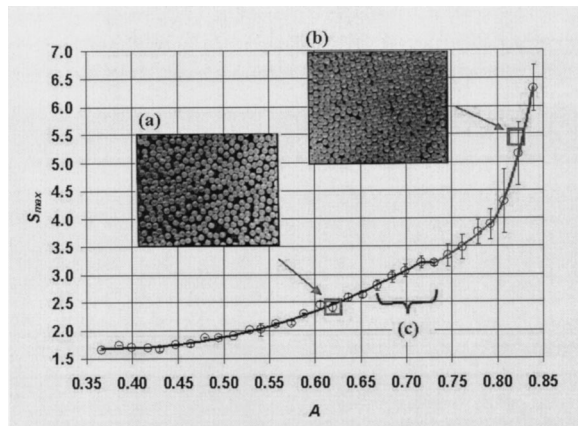


FIG. 6. Comparison of  $S_{\max}$  vs  $A$  experimental data with the literature [8,9]. Insets are photographs of glass spheres on a glass plate (from Ref. [8]) corresponding to (a) liquidlike,  $A=0.62$ ,  $S_{\max}=2.42$ , and (b) transition from liquidlike to solidlike,  $A=0.82$ ,  $S_{\max}=5.45$ . Circles are our experimental data and squares are data in Ref. [8]. Bracket (c) is from the liquidlike to the solidlike transition range in Ref. [9] ( $A=0.67-0.73$ ).

ment's  $S(Q)$  derived from the Fourier transform of the  $g(r)$ . The  $S(Q)$  show oscillatory decay, and the oscillation amplitude is more pronounced as  $A$  increases. A split appears in the second maximum between  $A=0.77$  and  $A=0.84$ . The split occurring at the second peak is characteristic of triangular-lattice formation [1,18,29,30]. From the observation of  $S(Q)$ , we know that there is particle structure assembly that is associated with an increasing  $A$ . We plot  $S_{\max}$  vs  $A$  in Fig. 4 to quantify the coverage of the particles that starts this structural transition [31]. The  $S_{\max}$  monotonically increases with the increasing area fraction. A small plateau appears at approximately  $S_{\max}=3.2$  and  $A=0.72-0.73$ , which indicates the transition in the particle structure (from liquidlike to triangular-lattice crystal-like). The curve shows large scatterings after  $S_{\max}=4$  ( $A=0.80$ ). We quantify the sixfold symmetry formation with a graph of  $G_6$  vs  $A$  [34] in Fig. 5 [the triangular-lattice construction is indicated by the split of the second peak in the  $S(Q)$ ]. It also has a small plateau and a scattering region in about the same area fraction range as that of  $S_{\max}(A)$ . The flat region at approximately  $G_6=0.32$  and  $A=0.70-0.72$  characterizes a structural transition. A fluctuation of  $G_6$  was observed in the  $0.74 < A < 0.81$  region. This fluctuation of  $S_{\max}(A)$  and  $G_6(A)$  requires more study. A possible explanation of the fluctuation is the existence of the “structural transition region” from a disordered structure to an ordered structure.

We compared our two-dimensional hard-sphere experimental data with that found in the literature. Turnbull and Cormia [8] conducted a simple two-dimensional experimental model by putting glass spheres on a glass plate. The uniform hard spheres moved steadily and at random. We quantitatively analyzed the two photographs given by Turnbull and Cormia in Figs. 6 and 7. We calculated  $S_{\max}$  and  $G_6$  in these two figures and compared them with our experimental results. Figure 6 of  $S_{\max}(A)$  and Fig. 7 of  $G_6(A)$  show that Turnbull and Cormia's data (4 mm diameter glass particles on a glass surface, marked as squares) are in good agreement

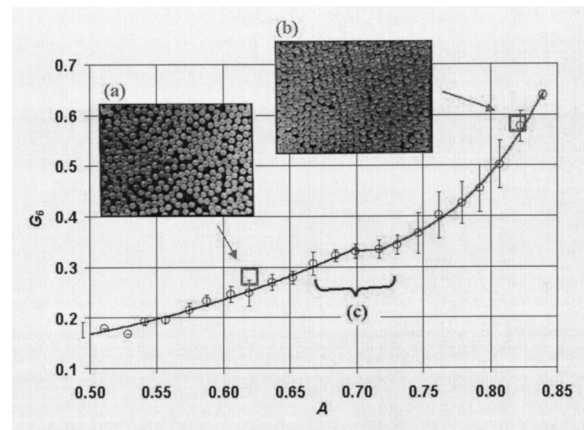


FIG. 7. Comparison of  $G_6$  vs  $A$  experimental data with the literature [8,9]. Insets are photographs of glass spheres on a glass plate (from Ref. [8]) corresponding to (a) liquidlike,  $A=0.62$ ,  $G_6=0.28$  and (b) transition from liquidlike to solidlike,  $A=0.82$ ,  $G_6=0.58$ . Circles are our experimental data and squares are data in Ref. [8]. Bracket (c) is from the liquidlike to the solidlike transition range in Ref. [9] ( $A=0.67-0.73$ ).

with our results (1.59 mm diameter steel particles on a silicon wafer surface). The first photograph that the authors argued is liquidlike has an area fraction of 0.62,  $S_{\max}$  is 2.42 (Fig. 6) and  $G_6$  is 0.28 (Fig. 7). The authors argued for the “transition from liquidlike to crystal-like” in the second photograph, where the area fraction is 0.82,  $S_{\max}$  is 5.45 and  $G_6$  is 0.58. The authors indicated the model exhibits a “gaslike” structure at a low sphere density. The structure becomes more “liquidlike” as the sphere density increases and then “crystallization” occurs.

Pieranski *et al.* [9] used another 2D hard-sphere model in their experiments. They used steel particles which have similar size to ours but spread them on a plastic surface. Tata *et al.* [11] experimented with a similar system of steel particles spread on a plastic surface; the steel particles acquired positive charges and left negative charges on the dielectric plastic surface. Pieranski *et al.* argued the structural transition from a liquidlike to a crystal-like structure happened at an area fraction of  $A=0.67-0.73$  (marked as bracket in Figs. 6 and 7). Our results showed the structural transition occurred at about  $A=0.70-0.73$  for the plateau region in  $S_{\max}(A)$  and  $G_6(A)$ . We cannot compare the results of  $S_{\max}$  and  $G_6$  because they only provided the photographic images of trajectories and the pair distribution function. One reason for the shift of their transition region from ours may be due to the presence of charges on the steel particles and the surface of plastic plate. The effective volume of a charged sphere is higher than that of a hard sphere, so we expect the particle structure of this charged system to be more ordered than a hard-sphere system. As a result, the structural transition for charged spheres is at lower area fraction than that of hard-sphere systems.

In order to understand the particle structural transition, we conducted a Monte Carlo simulation in the hard-disc system. Figure 8 shows the structure factor  $S(Q)$  obtained from Fourier transform of radial distribution function  $g(r)$  at several area fractions. Starting from area fraction  $A=0.69$ , the sec-

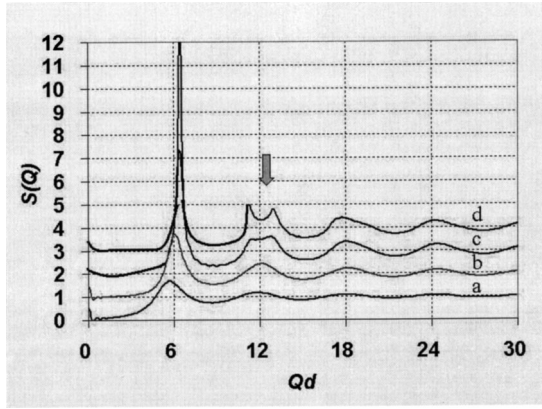


FIG. 8. Structure factor of 2D hard spheres by Monte Carlo simulation at different area fractions of  $A$ . Curves  $a$ ,  $b$ ,  $c$ , and  $d$  correspond to  $A=0.45, 0.60, 0.69, 0.71$ , respectively. Curves  $b$ ,  $c$ , and  $d$  are shifted vertically for clarity. The arrow shows the appearance of a triangular lattice.

ond peak exhibits a bump and gradually splits into two peaks with the increasing area fraction. The bump formation and split in the second peak is characteristic of triangular-lattice-order building [1,18,29,30]. The particles appear to have a structural transition from the disordered structure to the ordered structure (fluid-solid phase transition in literature [10,22]), as seen from the curves of structure factor versus particle coverage. Figure 9 shows the trend of  $S_{\max}$  as a function of the area fraction,  $A$ .  $S_{\max}$  increases monotonically with the increasing  $A$ .  $S_{\max}$  shoots up sharply when  $A$  reaches 0.69 and is accompanied with large scatterings. Tata *et al.* have argued that the particles are experiencing a structural transition when the slope of  $S_{\max}(A)$  suddenly changes [31].

The hard disc in Monte Carlo simulations built a triangular lattice at  $A=0.69$ , where the bump and splitting of  $S(Q)$  began (Fig. 8) and the slope of  $S_{\max}(A)$  suddenly increased (Fig. 9). In order to compare our results with computer simulation data in literature, we calculate the 2D pressure from the data  $g_{\max}(A)$  according to the following “equation of state” for 2D hard spheres [25,36]:

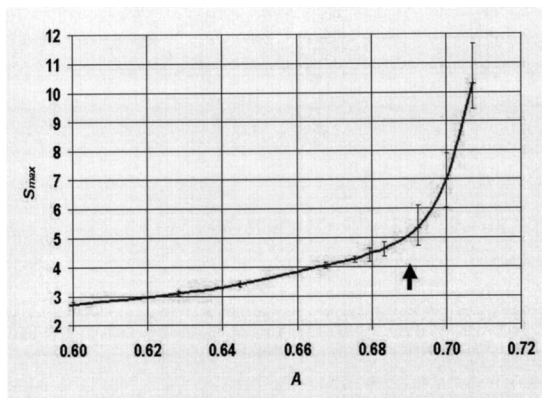


FIG. 9.  $S_{\max}$  vs  $A$  of 2D hard spheres by Monte Carlo simulation.  $S_{\max}$  shoots up sharply when  $A$  reaches about 0.69 and is accompanied with large scatterings (indicated by the arrow).

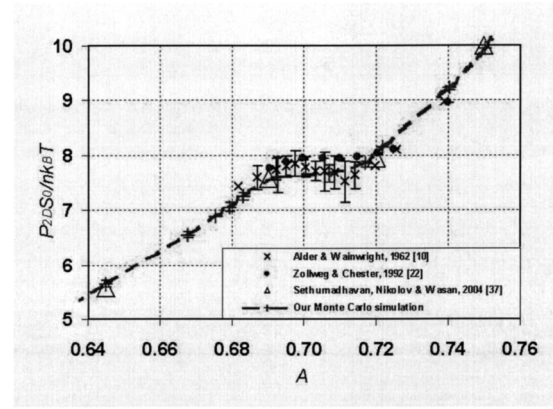


FIG. 10. 2D equation of state compared with the literature [10,22,37] based on computer simulations. The structural transition occurs at around  $A=0.69-0.71$ . The  $S_0$  is the system area of  $n$  particles at closed packing of triangular lattice,  $S_0=(\sqrt{3}/2)nd^2$ .

$$P_{2D} = \rho k_B T (1 + 2A g_{\max}), \quad (3)$$

where  $P_{2D}$  is the 2D pressure and  $g_{\max}$  is the first peak amplitude of  $g(r)$ . We summarize our results and others from the literature [10,22,37] in Fig. 10. Our computer simulation results are in good agreement with those from the literature. We know that the transition occurs at around  $A=0.69-0.71$ . For the narrow transition region with higher fluctuation, one can interpret it as the possibility of the occurrence of hexatic phase, which was predicted in KTHNY theory.

The experimental disorder-order transition occurs in the region of plateau and scattering region ( $A=0.70-0.82$ ) in  $S_{\max}(A)$  and  $G_0(A)$ . The existence of the transition region is a result of the coexistence of voids (dislocations) and the particle order. These dislocations were produced in the way we conducted the experiment. This may cause the formation of hexatic structure (KTHNY theory). As shown in some region of Fig. 2(B), even if we have a perfect ordered structure of 2D triangular lattice in the particle image, it can form a dislocation structure by missing some particles inside. The two-stage melting theory is on phase transition, driven by thermodynamics stability; the structural transition observed in our study is driven by mechanical equilibrium. The dislocations in particle structure slowly disappear with increasing particle area fraction during the transition region. At this moment, we cannot quantify the type of this transition region.

We compare the radial distribution function,  $g(r)$ , between the Monte Carlo simulation and experimental results at two different area fractions of  $A=0.67$  and  $A=0.75$  in Fig. 11. The inset snapshots represent the particle configurations in these coverage for experiment and simulation. The detail analysis of Fig. 11(A) shows agreement between experiment and simulation at the low area fraction of  $A=0.67$ . At the high area fraction of  $A=0.75$  as shown in Fig. 11(B), the  $g(r)$  of Monte Carlo simulation has more oscillatory peak and larger peak amplitude than the experiment. The split in the second peak indicates that the particles form a hexagonal packing in Monte Carlo simulation at  $A=0.75$ , but the experimental results do not show such a split. The snapshot for experimental particles depicts a lot of dislocations (marked

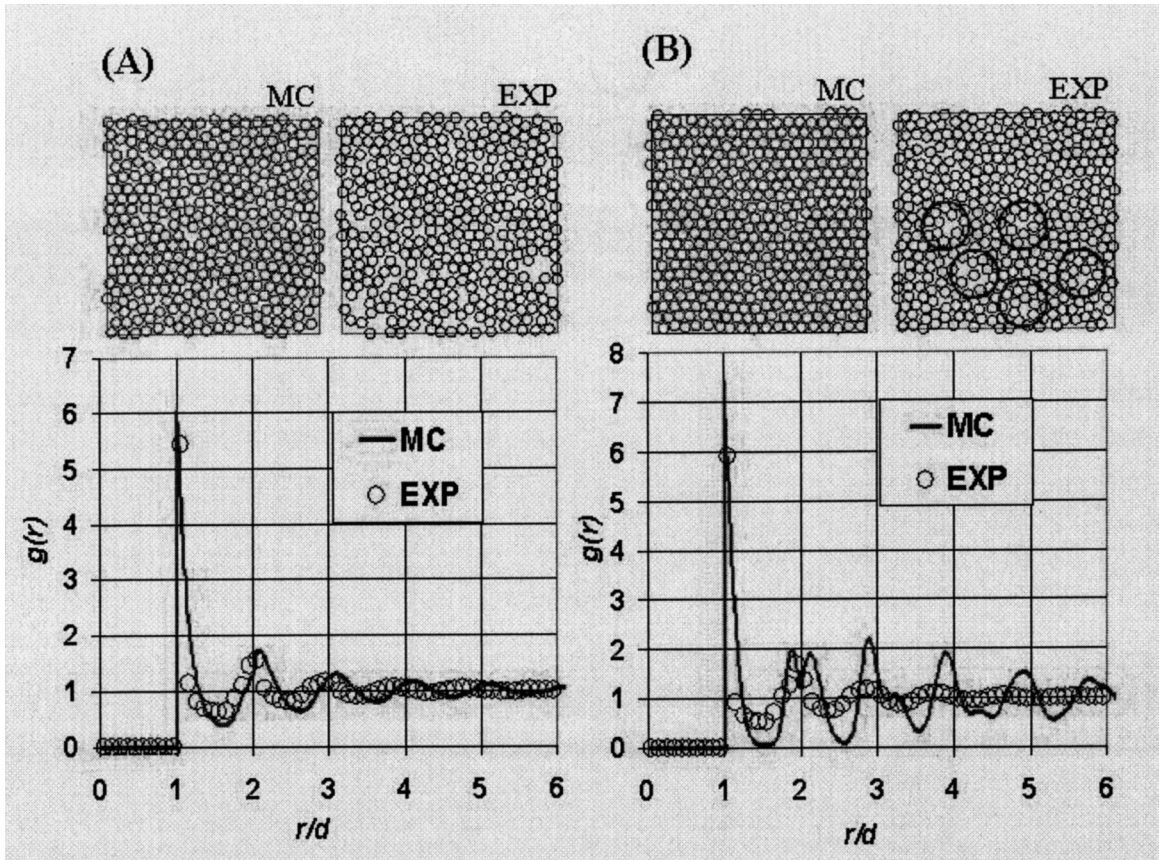


FIG. 11. Comparison between experiment and Monte Carlo simulations in particle configuration and radial distribution function at two different area fractions, (A)  $A=0.67$ , (B)  $A=0.75$ . The particle configurations are shown with dimension of  $20d$  by  $20d$ . The circled areas in the experimental configuration of (B) indicate the dislocations.

by the drawn circles), which are absent in simulation.

The discrepancy between the experimental and Monte Carlo results at high particle coverage is due to the manner how the particle structure was formed. The particle packing evolution was allowed during the shaking movement. Since the shaking was applied on the whole system instead of on an individual particle, we moved all the particles at the same time [38]. However, each particle moves individually when we did computer simulation; the particle would find place where the algorithm determined its minimum energy. When we conducted experiment at low area fraction, the particles have more space to move, therefore have higher possibility to find the place with low energy. However, at high area fraction, when we conducted the experiment, the particles had less freedom and less possibility to find place with low energy. As a result, particles are less structured compared with those in Monte Carlo simulation.

Shaking the platform is a requirement for a “driven” granular system [16], which supplies the particles kinetic energy lost through friction and sustains the system in a mechanic stability. Besides creating the particle movement, shaking platform also serves another important role of enabling particles to explore the configuration space [11]. The experimental particles are driven by mechanic stability; whereas particles in the Monte Carlo simulation are driven by thermodynamic consideration. Since the shaking was applied on the whole system instead of on an individual par-

ticle, we moved all the particles at the same time [38]. The granular particles have the tendency to form “a rather cold clump of material in a correlated motion” [14] due to their failure in “equipartition of energy” [39]. Similar to the observation of Straßburger and Rehberg [18], particle clustering and dislocation in our experiment became more pronounced at higher area fractions.

## VI. CONCLUSIONS

We investigated the two-dimensional hard-sphere structural transitions by conducting granular experiments and the Monte Carlo simulations. The second peaks of  $S(Q)$  gradually split, indicating the particles are forming a triangular lattice. We quantified the particle coverage at which the structural transition region occurs by observing the curves of  $S_{\max}(A)$  and  $G_6(A)$ . The flat parts occurring at both curves identify the structural transition occurring at about  $A=0.70-0.73$ ,  $S_{\max}=3.2$  and  $G_6=0.32$ . Afterwards, the curves show steep increases accompanied with a large amount of scattering.

Our experimental results are in good quantitative agreement with the 2D hard-sphere experiments in Ref. [8]. The experimental data for the order parameters,  $S_{\max}$  and  $G_6$ , were analyzed from their photographs and fall on our experimental curves of  $S_{\max}(A)$  and  $G_6(A)$ . Pieranski’s [9] 2D ex-

periments also show good qualitative agreement with our results by introducing the concept of effective volume for charged particles. Straßburger and Rehberg's [18] experiments have similar particle clustering and dislocation as observed in our experiment at higher area fractions.

Our experimental and the Monte Carlo simulation results for  $g(r)$  show good agreement at low area fractions. At high area fraction, the particles in the experiments form more clusters and vacancies than the particles in Monte Carlo simulations, which were created in experiment with shaking the platform. We moved all the particles at the same time

when shaking the whole system; in contrast to each particle moving individually in simulation. At high area fraction, the particles have less freedom and less possibility to find place with low energy. As a result, particles are less structured compared with those in Monte Carlo simulation.

#### ACKNOWLEDGMENTS

The authors thank A. Trokhymchuk for helpful discussion. The financial support provided by the National Science Foundation is gratefully acknowledged.

- 
- [1] D. R. Nelson, in *Phase Transitions and Critical Phenomena*, edited by C. Domb and J. L. Lebowitz (Academic, London, 1983), Vol. 7.
- [2] K. J. Strandburg, in *Bond-Orientational Order in Condensed Matter Systems*, edited by K. J. Strandburg (Springer, Berlin, 1992).
- [3] K. J. Strandburg, *Rev. Mod. Phys.* **60**, 161 (1988); M. A. Glaser and N. A. Clark, *Adv. Chem. Phys.* **83**, 543 (1993).
- [4] D. A. McQuarrie, *Statistical Mechanics* (Harper Collins, New York, 1976).
- [5] D. Frenkel and J. P. McTague, *Annu. Rev. Phys. Chem.* **31**, 491 (1980).
- [6] J. P. Hansen and I. R. McDonald, *Theory of Simple Liquids* (Marcel Dekker, New York, 1997).
- [7] J. A. Barker and D. Henderson, *J. Chem. Phys.* **47**, 2856 (1967).
- [8] D. Turnbull and R. L. Cormia, *J. Appl. Phys.* **31**, 674 (1960).
- [9] P. Pieranski, J. Malecki, W. Kuczynski, and K. Wojciechowski, *Philos. Mag. A* **37**, 107 (1978); P. Pieranski, *Am. J. Phys.* **52**, 68 (1984).
- [10] B. Alder and T. Wainwright, *Phys. Rev.* **127**, 359 (1962).
- [11] B. V. R. Tata, P. V. Rajamani, J. Chakrabarti, A. Nikolov, and D. T. Wasan, *Phys. Rev. Lett.* **84**, 3626 (2000).
- [12] H. M. Jaeger, T. Shinbrot, and P. B. Umbanhowar, *Proc. Natl. Acad. Sci. U.S.A.* **97**, 12959 (2000).
- [13] H. M. Jaeger, S. R. Nagel, and R. P. Behringer, *Rev. Mod. Phys.* **68**, 1259 (1996).
- [14] L. P. Kadanoff, *Rev. Mod. Phys.* **71**, 435 (1999).
- [15] A. Prevost, D. A. Egolf, and J. S. Urbach, *Phys. Rev. Lett.* **89**, 084301 (2002).
- [16] J. S. Olafsen and J. S. Urbach, *Phys. Rev. Lett.* **81**, 4369 (1998).
- [17] W. Losert, D. G. W. Cooper, and J. P. Gollub, *Phys. Rev. E* **59**, 5855 (1999).
- [18] G. Straßburger and I. Rehberg, *Phys. Rev. E* **62**, 2517 (2000).
- [19] I. Goldhirsch and G. Zanetti, *Phys. Rev. Lett.* **70**, 1619 (1993).
- [20] H. J. Herrmann, J.-P. Hovi, and S. Luding, in *NATO ASI Series* (Kluwer Academic, Dordrecht, The Netherlands, 1998), Ser. E, Vol. 350.
- [21] W. G. Hoover and F. H. Ree, *J. Chem. Phys.* **49** 3609 (1968).
- [22] J. A. Zollweg and G. V. Chester, *Phys. Rev. B* **46**, 11186 (1992).
- [23] H. Weber, D. Marx, and K. Binder, *Phys. Rev. B* **51**, 14636 (1995).
- [24] V. N. Ryzhov and E. E. Tareyeva, *Phys. Rev. B* **51**, 8789 (1995).
- [25] N. Metropolis *et al.*, *J. Chem. Phys.* **21**, 1087 (1953).
- [26] A. Rahman, *Phys. Rev.* **136**, A405 (1964).
- [27] R. J. Hunter, *Foundations of Colloid Science* (Clarendon, Oxford, 1989), p. 694.
- [28] H. T. Davis, *Statistical Mechanics of Phases, Interfaces, and Thin Films* (Wiley-VCH, New York, 1996), p. 665.
- [29] X. L. Chu, A. D. Nikolov, and D. T. Wasan, *J. Chem. Phys.* **103**, 6653 (1995).
- [30] G. H. Ristow, G. Straßburger, and I. Rehberg, *Phys. Rev. Lett.* **79**, 833 (1997).
- [31] B. V. R. Tata and A. K. Arora, *J. Phys.: Condens. Matter* **3**, 7983 (1991); **4**, 7699 (1992); B. V. R. Tata and N. Ise, *Phys. Rev. B* **54**, 6050 (1996); *Phys. Rev. E* **58**, 2237 (1998).
- [32] B. V. R. Tata, A. K. Arora, and M. C. Valsakumar, *Phys. Rev. E* **47**, 3404 (1993).
- [33] N. D. Mermin, *Phys. Rev.* **176**, 250 (1968).
- [34] B. Pouligny, R. Malzbender, P. Ryan, and N. A. Clark, *Phys. Rev. B* **42**, 988 (1990); H. Weber, D. Marx, and K. Binder, *ibid.* **51**, 14636 (1995); A. Huerta *et al.*, *J. Chem. Phys.* **120**, 1 (2004).
- [35] A. Huerta and G. G. Naumis, *Phys. Rev. Lett.* **90**, 145701 (2003).
- [36] F. Lado, *J. Chem. Phys.* **49**, 3092 (1968).
- [37] G. Sethumadhavan, A. Nikolov, and D. Wasan, *J. Colloid Interface Sci.* **272**, 167 (2004).
- [38] S. McNamara and S. Luding, *Phys. Rev. E* **58**, 813 (1998).
- [39] Y. Du, H. Li, and L. P. Kadanoff, *Phys. Rev. Lett.* **74** 1268 (1995).